10th ECCOMAS Thematic Conference on Computational Methods in Structural Dynamics and Earthquake Engineering M. Papadrakakis, M. Fragiadakis (eds.) Rhodes Island, Greece, 15-18 June 2025

SEISMIC FRAGILITY ASSESSMENT FOR WELDED STEEL MOMENT-RESISTING FRAMES UNDER ATMOSPHERIC CORROSION DETERIORATION

Devang B. Lad¹, Fabio Freddi¹, and Jayadipta Ghosh²

¹ Dept. of Civil, Environment and Geomatic Engineering, University College London Gower Street, London, United Kingdom e-mail: {devang.lad.21,f.freddi}@ucl.ac.uk

² Dept. of Civil Engineering, Indian Institute of Technology Bombay Powai, Mumbai, India {jghosh}@ iitb.ac.in

Abstract

Non-seismically designed steel building structures are typically characterised by limited ductility and may exhibit poor performance during seismic events. Furthermore, atmospheric corrosion can exacerbate their vulnerabilities, significantly diminishing their capacity. Corrosion deterioration depends on the exposure duration and environmental conditions and is associated with a high degree of variability and uncertainty. Seismic fragility curves facilitate the evaluation of increased failure probability by accounting for the combined effects of uncertainty in corrosion deterioration and seismic input variability. The present study examines the seismic performance of steel buildings under the combined effect of corrosion deterioration and seismic hazard. A set of three steel buildings considering different heights (i.e., 3-, 6-, and 9-storey) and designed according to pre-Northridge codes are adopted for case-study purposes. Corrosion modelling, considering uncertainty, under different corrosivity categories as per ISO 9223 is examined to derive the mass loss range over the service life of the building. Consequently, the probabilistic seismic assessment is conducted for the case-study steel frames using Incremental Dynamic Analyses (IDAs) through a suite of 30 ground motions, considering the earthquake input uncertainty. The case-study structure's global and local response parameters are monitored to develop fragility functions. Finally, a critical discussion on increased fragility comparing the three case-study frames is provided.

Keywords: Existing steel moment resisting frame, Atmospheric corrosion, Fragility Curves, Local engineering demand parameters.

1 INTRODUCTION

The 1994 Northridge earthquake caused significant damage to steel moment resisting frames (MRFs), leading to brittle fractures at the beam-column joints and damaging more than 150 buildings [1]. Post-earthquake investigations on steel MRFs, prevalent in the seismically active regions of the United States (US), revealed weak panel zones, brittle welds, limited ductility, and insufficient energy dissipation capacity [2]. Moreover, these existing low-code (*i.e.*, designed prior to modern seismic codes) steel MRFs experience atmospheric corrosion deterioration during their service life, thereby exacerbating the seismic performance. Corrosion deterioration is identified as a major cause of damage to buildings and infrastructures globally, leading to mass loss (primary effect) and degradation in mechanical properties (secondary effects). Particularly for steel buildings, experimental studies [3,4] highlighted that corrosion deterioration adversely affects lateral strength and ductility, increasing the risk of seismic failure, endangering lives, and causing economic losses.

Seismic fragility curves help evaluate the structure's failure probability for a given seismic intensity level, taking into account record-to-record variability. These tools have been used in several research studies to evaluate the evolution with time (*i.e.*, time-dependent fragility curves) of several structural systems, mainly bridges and reinforced concrete (RC) structures [5,6]. Only a limited amount of studies focused on steel buildings. For instance, Lekeufack *et al.* [7] showed increased exceedance probability of seismic failure for steel MRFs in coastal atmospheric corrosive environments. Di Sarno *et al.* [8] investigated the effects of corrosion deterioration on the seismic performance of petrochemical building structures exposed to varying corrosive environments, showing a significant increase in the global demand parameters. Shekhar *et al.* [6] investigated the influence of corrosion on the seismic performance of lowcode RC building structures and emphasised the importance of monitoring local parameters.

Similarly, Lad *et al.* [9,10] assessed the seismic fragility of a 3-storey low-code steel MRF under atmospheric corrosion deterioration, emphasizing the need to monitor local component responses, including considerations on the beam-column joints, which are characterised by a lack of capacity design considerations [2]. The results highlighted a notable increase in both global and local responses, as well as the failure probability. Additionally, it was found that the local components governed the system failure fragility for low-code steel MRFs. However, the developed fragility curves are time-dependent and building-specific and hence, have limited applicability to other sites and building structures. To overcome this limitation, the present study extends the previous work [9,10] and develop generic mass-loss-based fragility functions for low-code steel MRFs, considering different configurations and incorporating uncertainty in corrosion and earthquake input.

The present work evaluates the seismic fragility of three steel MRFs from the SAC FEMA project. These steel MRFs, have heights of 3-, 6-, and 9-storey and were designed using pre-Northridge design codes (low-code). Corrosion deterioration is accounted for by considering different levels of mass loss, rather than assuming a single location and corrosivity category. This strategy aims to provide more general results with wider applicability. Mass losses are assumed considering varied atmospheric corrosivity categories as defined in ISO 9223 [11]. Corrosion uncertainty is accounted for, and a standard deterioration level (or range) is defined to encompass different ageing times. Uniform corrosion is considered for columns and panel zones, along with degradation in steel's mechanical properties. A Finite Element (FE) model of the as-built and corroded frames is developed in OpenSees [12] for the non-linear dynamic analysis. Incremental Dynamic Analyses (IDAs) are conducted using a suite of 30 ground motion records to account for the record-to-record variability while monitoring local and global component responses. The results of IDA help develop fragility curves at both system and

component levels. Finally, a comparison of the seismic performance and evolution of the fragility curves for the three case-study frames is discussed. The derived mass-loss-based fragility functions for low-code steel buildings with varied storey heights represent a first step toward seismic risk assessment for corroded structures at a regional scale [6].

2 ATMOSPHERIC CORROSION DETERIORATION

Atmospheric corrosion deterioration primarily leads to the formation of rust on steel members. The electrochemical process in which iron is converted into rust results in variable thickness loss or mass loss (η) of the steel. The study assumes uniform corrosion in steel to consider for worst-case scenarios. Total damage in the form of cross-sectional mass loss over a period is quantified using the corrosion rate. The corrosion rate (r_{corr}) reflects the corrosion kinematics of the environment for the exposed duration. ISO 9223: 2012 [11] classifies the corrosive environment into six categories (C1-CX), and, for carbon steel, it suggests a first-year corrosion rate [or r_{corr} in μ m/y or g/(m²×y)] range for each category. The classification incorporates different corrosion influencing factors and quantifies r_{corr} using regression models over long-term recorded experimental datasets [11]. These regression models represent the atmospheric corrosion model used to quantify the corrosion damage.

The ISO 9224: 2012 [13] suggests evaluating corrosion deterioration as follows:

$$d(t) = r_{corr} \times t^{B} \qquad \dots (t < 20 \text{ y})$$

= $r_{corr} \times [20^{B} + B \times (20^{B-1}) \times (t-20)] \dots (t \ge 20 \text{ y})$

where, d(t) is the thickness loss of steel's cross-section, r_{corr} is the first-year corrosion rate, B is the time exponent coefficient, and 20 years is considered as stabilization time. Previous studies by the authors [10], estimated the corrosion damage for C3 to CX corrosivity categories for a 50-year exposure period, where the average values of r_{corr} provided in ISO 9223: 2012 [11] were adopted along with the time exponent, B=0.523. In the present study, a 75year exposure period is considered along the uncertainty in r_{corr} and B values as defined in ISO 9223: 2012 [11]. Figure 1(a) shows the evolution of mass loss $[\eta(t)]$ over 75 years for C3 to CX categories in internal columns of the 3B building. A significant variation is observed in the steel's mass loss over a 75-year exposure period; for instance, η =3.7% for C3 category to η =27% for the CX category. However, the current study aims to incorporate corrosion uncertainty and develop time-independent fragility curves. Thus, instead of evaluating timedependent corrosion mass loss, a pre-defined mass loss of 5% to 30% is assumed for seismic fragility assessment. Fragility curves for a predefined mass loss essentially delink the results from time-based corrosion losses. Corrosion uncertainty can be easily incorporated by evaluating the mean mass loss for a t-year period and subsequently adopting the relevant fragility curve for risk assessment.

Furthermore, the secondary effects of corrosion deterioration include the degradation of steel's mechanical properties and are assessed according to Wang *et al.* [3]. The degradation in mechanical properties is related to mass loss as follows:

$$f_{\rm V}[\eta(t)] = f_{\rm V0} \times [1 - 1.09 \times \eta(t)]$$
 (2)

where f_{y0} and $f_y[\eta(t)]$ are the initial and degraded yield strength of the steel material, respectively. For mass losses, $\eta(t)$, of 5, 10, 15, 20, 25, and 30%, the corresponding degradation in f_y/f_{y0} are 0.945, 0.89, 0.836, 0.782, 0.73, and 0.68. For illustration purposes, Figure 1(b) shows the degradation in f_y over 75 years for C3 to CX categories as per Eq. 2 for the grid B-storey 0 column in the 3-storey building.

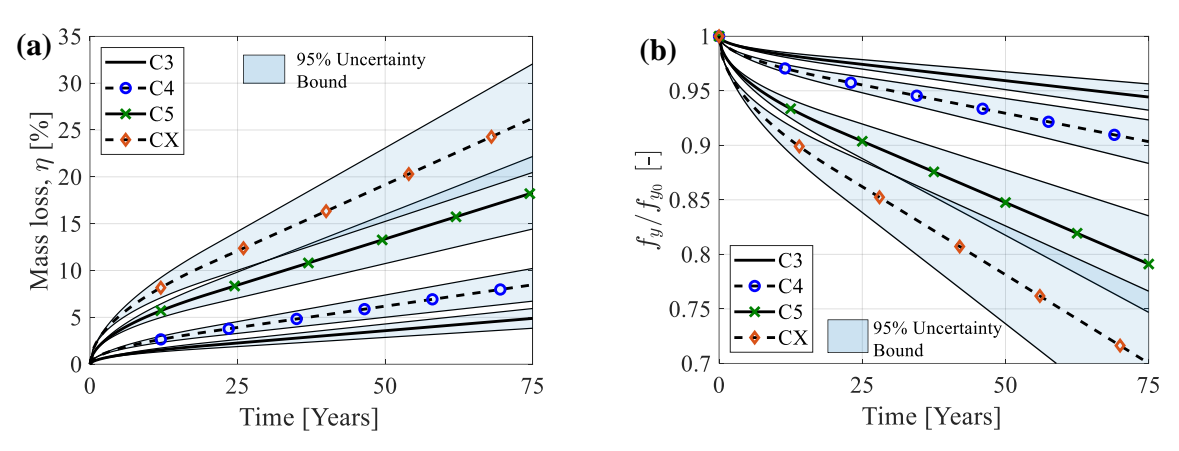


Figure 1: (a) Corrosion mass loss (η) , (b) Yield strength (f_y/f_{y0}) reduction for the grid B-storey0 column of 3-storey building.

3 CASE-STUDY BUILDINGS DESCRIPTION

The pre-Northridge Boston's buildings, with 3- and 9-storey from the SAC-FEMA project are used for case-study purposes [14]. Additionally, a 6-storey steel building of similar characteristics is adopted from Gutiérrez-Urzúa & Freddi [2]. The considered 3-, 6- and 9-storey steel MRFs represent low and mid-rise steel structures with regular plan-elevation distributions. In addition, these case-study structures are characterised as low-code, being designed in the absence of modern seismic codes, and lacking capacity design considerations. For brevity, they are referred to as 3B, 6B, and 9B buildings. The plan view for buildings 3B is shown in Figure 2(a), while for 6B, and 9B is shown in Figure 2(b), while Figure 1(c) to (e) show the elevation for 3B, 6B, and 9B, respectively.

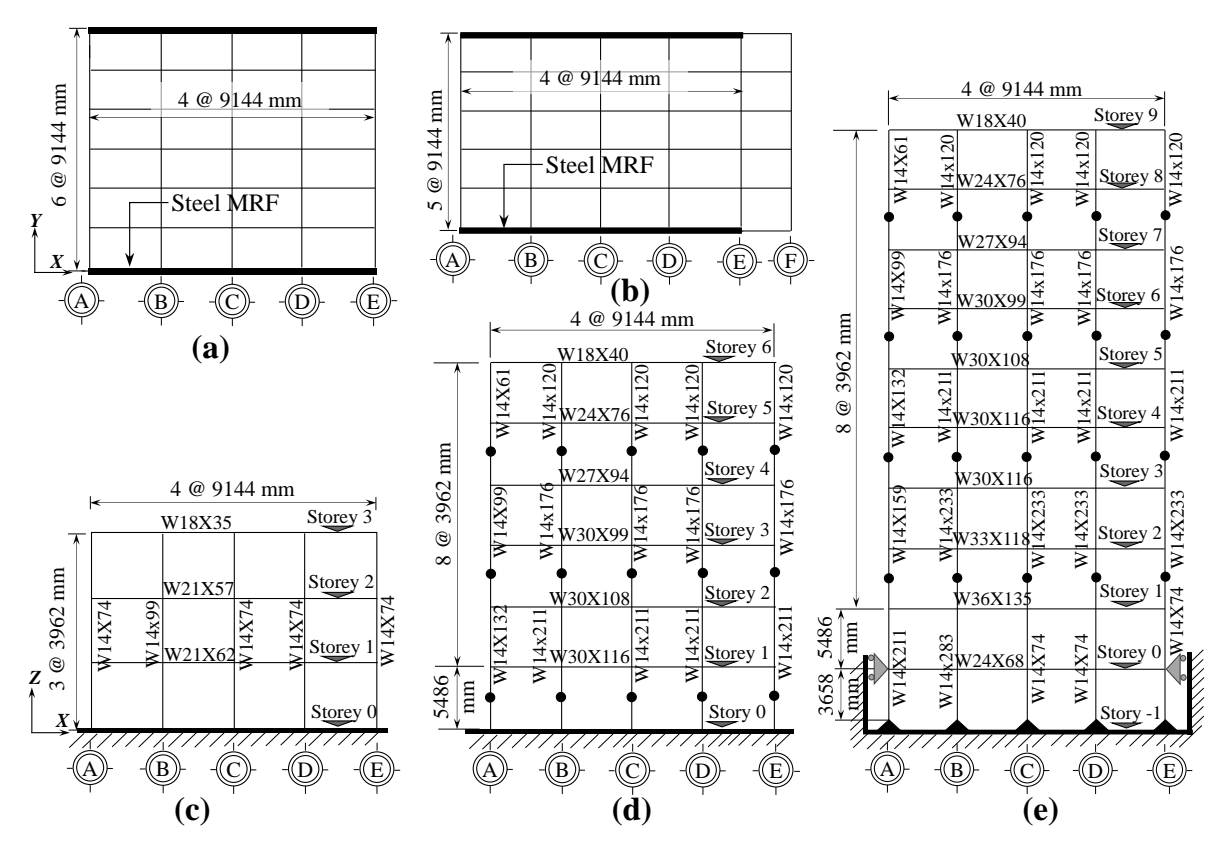


Figure 2: Case-study structure: Plan view of (a) 3B, (b) 6B and 9B. Elevation view of (c) 3B, (b) 6B, and (c) 9B.

For all the frames, the lateral loads are resisted by the perimeter steel MRF denoted using the thick line in the plan view. Only half of each storey mass is assigned in the FE model for a single perimeter frame. The original 9B building design is slightly modified by eliminating the semi-pinned external span (from E to F), as its contribution to lateral strength and stiffness is negligible. Instead, it is treated solely as part of the gravity system. Furthermore, the 6B building is directly adopted from Gutiérrez-Urzúa & Freddi [2]. The seismic mass for each building is listed in Table 1. The present study assumes these buildings are constructed on soft rock (Type BC) in Los Angeles, California, United States, with all case-study structures classified under seismic risk category II as ASCE 7-16 [15].

The steel MRFs are assumed to be built along Los Angeles' coastline in urban environment to represent varying corrosivity categories as per ISO 9223:2012 [11]. For simplicity, the study assumes no corrosion protection through surface painting, and the steel is exposed to atmospheric agents. As discussed in Section 2, a pre-defined mass loss of 5%-30% in columns is assumed to occur for all steel MRFs over different ageing times under varying corrosivity categories. Consequently, the analysis includes the as-built frame along with corroded frames experiencing 5, 10, 15, 20, 25, and 30% mass loss in columns.

Building 3B		Bu	Building 6B		Building 9B	
Story	Mass [ton]	Story	Mass [ton]	Stor	y Mass [ton]	
1	956.64	1	1009.19	1	1009.19	
2	956.64	2 to 5	991.73	2 to	8 991.73	
3	1035.41	6	1069.29	9	1069.29	

Table 1: Seismic masses of each storey for buildings 3B, 6B and 9B, respectively [2,16].

4 FE MODELLING OF AS-BUILT AND CORRODED FRAME

Figure 3 shows the modelling strategy adopted for the case-study frames in OpenSees [12]. A 2D non-linear FE model of each case-study structure 3B, 6B, and 9B is developed. Columns are modelled through a distributed plasticity approach, while beams are modelled using a lumped plasticity approach. Plastic hinges are defined according to the model proposed by Lignos and Krawinkler [17] and modified as per Zareian and Medina [18]. The yield strength (f_y) and elastic modulus (E) of the as-built frame are equal to f_y =344.74 MPa and E=199.95 GPa, respectively. The nominal value of f_y is increased by 10% to account for the material overstrength. A damping ratio of 3% is adopted using the mass and stiffness proportional damping. Column bases are considered fixed for 3B and 6B, whereas pinned for 9B as discussed in [2,16]. The interactions with gravity frames and P- Δ effects are represented through a leaning column. Additional information on the modelling strategy is available in [2,16].

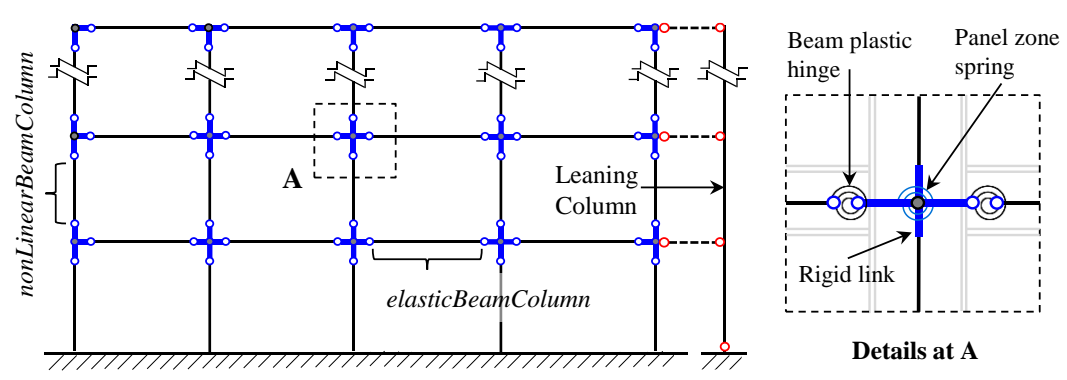


Figure 3: Numerical modelling strategy for the case-study 3B frame in OpenSees [12].

The beam-column joints are considered to be welded and fully restrained as per the original design. The panel zone location is modelled using rigid links equivalent to the depth of the column and beam sections, as shown in Figure 3. The flexibility in the panel zones is accounted for at the beam-column joints, as shown in Figure 4. For this, a single *zeroLength* element is modelled at the centre, assigned with a newly proposed panel zone shear strength model (or backbone curve through *HystereticSM* material) by Skiadopoulos *et al.* [19]. The adopted new model effectively captures both shear and bending deformation in the series of the web panel. Figure 5(a) to (d) shows the mechanical model, corresponding FE modelling strategy at beam-column joint, and backbone curve assigned to the panel zone spring.

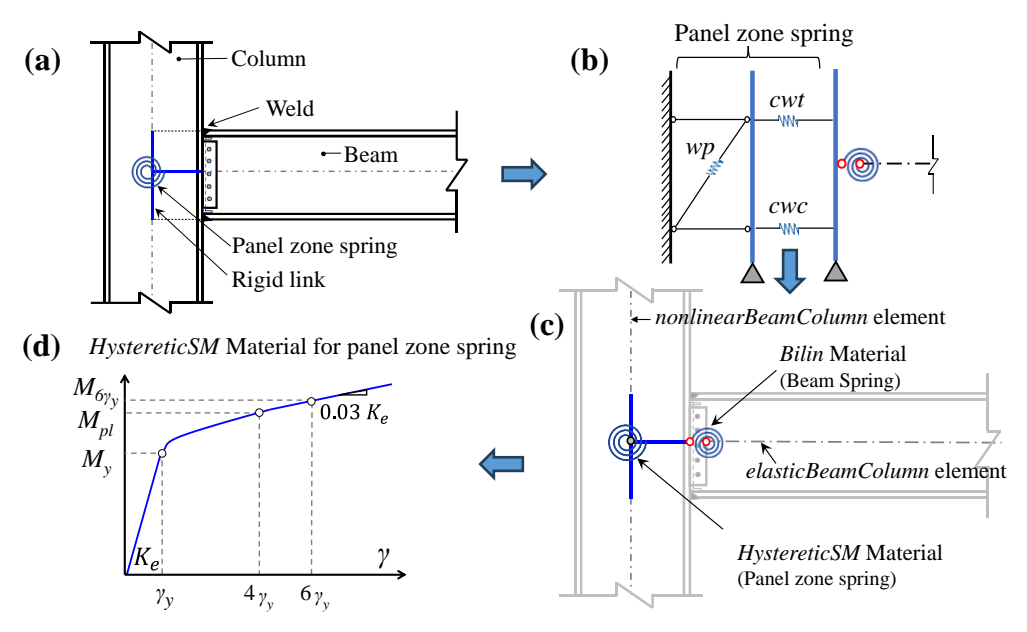


Figure 4: Beam-column joint modelling strategy— (a) Connection details (b) Mechanical model for panel zone, (d) FE modelling in OpenSees, and (e) backbone curve for *HystereticSM* material for the panel zone spring. (*cwc*-column web in compression; *cwt*—column web in tension; & *wp*—web panel in shear and bending).

The FE models of the corroded frames representing 5% to 30% mass loss (with 5% increment) are developed in OpenSees [12]. For this, uniform thickness loss [d(t)] corresponding to each mass loss level is applied in all column sections through newly developed FE model. This approach accounts for the primary effects due to corrosion deterioration. The secondary effects, degradation in the mechanical properties, are accounted for by modifying the yield strength (f_y) as per Eq. (2). The rotational spring properties for panel zones are estimated, accounting for the primary and secondary corrosion losses. In this study, corrosion in beams is neglected. This assumption is justified by the fact that beams are partially protected by the slab and, thus, are in a low-corrosive environment. Moreover, being non-seismically designed buildings characterised by weak panel zones and strong beam-weak column mechanisms, beam deterioration has an insignificant impact on the seismic capacity of the frames.

5 SEISMIC PERFORMANCE ASSESSMENT

5.1 Engineering Demand Parameters (*EDP*s) and code-based capacity limits

There is no well-established relationship between local failure and global Engineering Demand Parameters (*EDP*s) for low-code structures [16]. Therefore, the current study adopts both local and global *EDP*s for fragility assessment. The maximum interstorey drift ratio

(MIDR) is selected as global EDP, while column rotation (θ_c), panel zone shear strain (γ), and beams' rotation (θ_b) as local EDPs.

The damage level estimation (limit states, *LS*, or acceptance criteria) follows the recommendations of ASCE 41-17 [20]. For each local *EDPs*, ASCE 41-17 categorizes three limit states (*LSs*) - (i) *LS1* (Immediate occupancy), (ii) *LS2* (Life safety), (iii) *LS3* (Collapse prevention). The code explicitly defines capacity limits for each *EDP* and *LS* in terms of plastic rotation for each component level. Conventionally, for local *EDPs*, deformation-based capacity parameters can be used as limit state thresholds, as discussed in earlier studies [9,10]. Table 1 enlists the limit states defined in terms of component-level plastic rotation capacity limits. For additional details, the readers can refer to Gutiérrez-Urzúa *et al.* [16]. For the global *EDP*, *MIDR*, the limit states adopted are equal to 0.7% (LS1), 2.5% (*LS2*) and 5% (*LS3*) according to ASCE 41-07 [21].

Floment	Dimensionless	Plastic rotation capacity limits			
Element	axial load limits	LS1	LS2	LS3	
Columns* $[\theta_c]$	$ v_{\rm G} < 0.6$	0.5a	0.75b	b	
Panel zones $[\gamma]$	$ v_{\rm G} < 0.4$	1. γ _y	12. γ _y	12. γ _y	

Notes: * 'a' and 'b' are defined in Table 9-7.1 of the ASCE 41-17 [20]. γ_y – panel zone yield rotation capacity. v_G – dimensionless axial load ratio.

Table 2: Component-level plastic rotation (or local EDPs) capacity limit states (LS) as per ASCE 41-17 [20].

5.2 Intensity Measure (*IM*)

Corrosion deterioration leads to mass loss of member sections, resulting in a slight reduction in the stiffness of the entire structure. Consequently, time period elongation is observed for the corroded frame over its service life [9]. Thus, to facilitate the comparison of the seismic response of the as-built vs. the corroded frame, the average spectral acceleration (Sa_{avg}) between the fundamental time periods of the as-built ($T_{1,as\text{-built}}$) and corroded ($T_{1,c}$) frames is adopted as Intensity Measure (IM). Sa_{avg} is evaluated using the geometric mean of accelerations between $T_{1,as\text{-built}}$ and $T_{1,c}$ of most corroded frame [6,9]. For the current study, corroded frame corresponding to 30% mass loss (η) represents the most flexible frame. Table 3 provides the $T_{1,as\text{-built}}$ and $T_{1,c}$ for each case study buildings. The adopted Sa_{avg} allows direct comparison of the fragility curves for the as-built and corroded frames.

Building 3B	T_1 [sec]	Building 6B	T_1 [sec]	Building 9B	T_1 [sec]
As-built	1.93	As-built	2.41	As-built	3.42
$\eta = 30 \%$	2.18	$\eta = 30 \%$	2.56	$\eta = 30 \%$	3.64

Table 3: Fundamental time period in seconds for 3B, 6B, and 9B for the as-built and corroded frame with 30% mass loss.

5.3 Ground Motion and Incremental Dynamic Analyses (IDAs)

Nonlinear time history analyses (NLTHAs) are performed using a suite of 30 recorded ground motions (GMs) selected from the NGA-WEST2 database, accounting for record-to-record variability. These include non-pulse type far-field GMs with moment magnitude (M_w) ranging from 5 to 7.4. As per ASCE 7-22 [22], the target spectrum is developed for Los Angeles, considering risk category II and site soil type BC. Subsequently, the GM records are scaled to match the target spectrum between the fundamental time periods of $0.2T_1$ of the asbuilt 3B frame and $1.5T_1$ of the 30% mass loss 3B frame. Finally, these 30 GM records are employed to conduct IDAs, where the system is subjected to a suite of scaled GMs with IM

spanning 0.1g to 1.0g. IDAs aid in capturing the complete range of structural responses, encompassing linear, nonlinear, and collapse stages. The structural response, recorded for local and global parameters at specific *IM* levels, allows generating the *EDPs-IM* pairs for fragility development.

5.4 Seismic Fragility Curves

Fragility curves are derived utilizing the *EDPs-IM* pairs for local and global *EDPs*. Demand sample corresponds to the maximum response recorded during each time-history analysis and among all components (*i.e.*, series arrangement of the components) for the chosen *EDP*. The maximum recorded response (or demand) is compared with the code-based capacity limits (Table 3-Section 5.2) to develop fragility curves. Fragility curves present the exceedance probability for a specified *LS*, conditional on a given *IM* level. It is important to highlight that the capacity values account for the corrosion deterioration as they are normalised/compared to yield-capacity parameters (*i.e.*, 'a' and 'b' parameters for column rotations, while γ_y for panel zone rotations, in Table 2) [9,10]. Numerical fragility curves are approximated by analytical lognormal curves obtained through least-square minimization. The component-level seismic fragility curves can be described as follows:

$$P(Demand \ge Capacity \mid IM) = P(\theta \ge C_{LS} \mid IM)$$
 (3)

where θ is the demand sample, C_{LS} is the capacity limit for each EDP and each LS, evaluated separately for as-built and corroded frames. Fragility curves for MIDR (global EDP) are derived similarly, but without incorporating reduction in capacity values due to corrosion as no guidance is available for this. Fragility results using the adopted methodology aids in integrating the uncertainty in seismic demand (*i.e.*, record-to-record variability), as well as the variation of demand-dependent and deterioration dependent capacity values. Figure 5 provides the seismic fragility curves for the as-built and corroded frames (10, 20 vs. 30 % mass loss) for panel zone rotations, (local EDP) and MIDR (global EDP) for 3B, 6B, and 9B. Concurrently, Table 4 reports the median (med) and dispersion (disp) of the lognormal fragility curves for the as-built and corroded frames (5, 10, 15, 20, 25, and 30% mass loss, η), as well as the percentile variations for LS3 only, for easier comparison with Figure 5. For the sake of brevity, fragility curves and corresponding parameters for column (θ_c) and beam rotations (θ_b) are not discussed as they do not influence the system fragility.

Figure 5(a) and (b) present seismic fragility curves of panel zone rotations, γ , (local EDP) and (b) MIDR (global EDP) for LS3 for building 3B. An increasing trend is observed with increasing mass loss (η) for both local and global EDP. The percentage variation of med values in Table 4 shows a similar increase of fragility with respect to mass loss of 25 and 30%. Conversely, for building 6B, the percentage variation in med values (Table 4) shows a smaller variation for the corresponding mass loss for both the EDPs. For instance, a 30% mass loss in 6B results in a 24.3% reduction in the *med* of panel zone rotation and a 12.1% decrease in med of MIDR. In addition, from the fragility curves of 6B for LS3 in Figure 5(c) and (d), it can be observed that MIDR does not show a consistent trend compared to panel zone rotations. Therefore, it can be concluded for 6B that the panel zone reflects a higher increased fragility versus the MIDR. Figure 5(e) and (f) show the fragility curves of panel zone rotations, γ , while Figure 5(b) shows the fragility curves for MIDR for LS3 for building 9B. Contrary to 3B and 6B, the panel zone do not show an increase in fragility up to 15% mass loss (Table 4). Also, MIDR shows approximately similar percentage variations in the med for 15 to 30% mass loss. However, for both the local and global EDP for 9B, the increase in fragility (or percentage variation in med) is smaller than the corresponding mass loss as reported in Table 4.

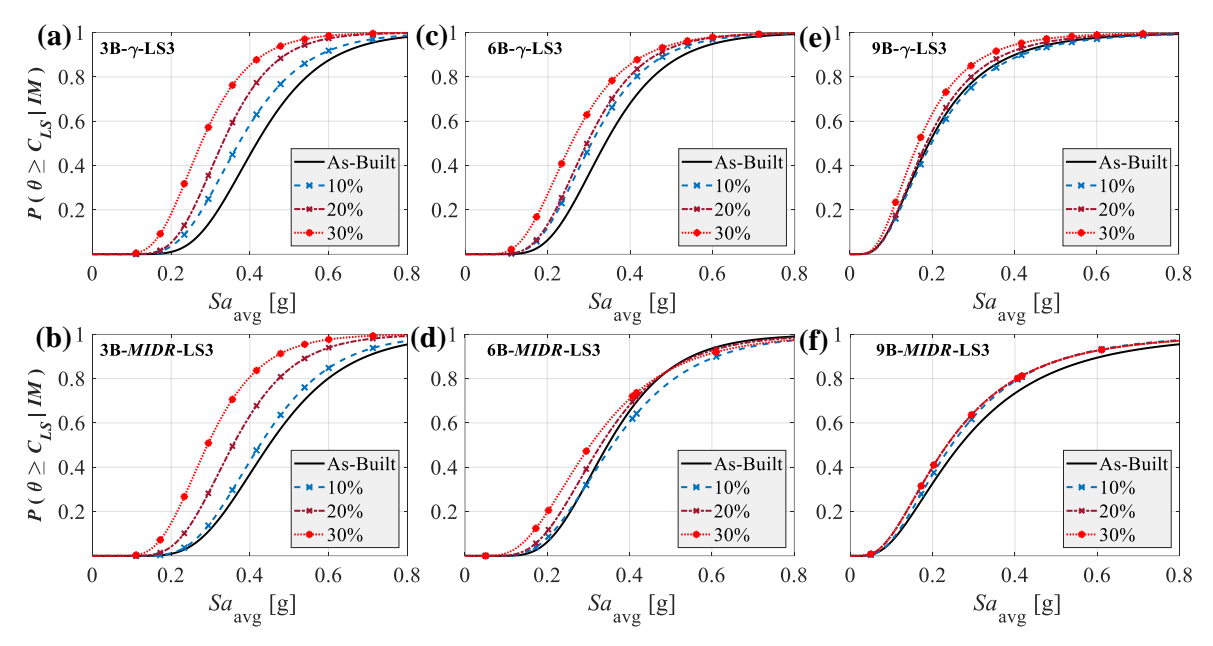


Figure 5. Fragility curves for the case-study structure- (a) panel zone rotations, γ , (local *EDP*) and (b) *MIDR* (global *EDP*) for the 3B building; (c) γ and (d) *MIDR* for the 6B building; (e) γ and (f) *MIDR* for the 9B building.

Nevertheless, for all three case study buildings, panel zone rotations govern the system fragility and show lower *med* values compared to global *EDP*. This finding is consistent with previous study by the authors [9,10]. From Figure 5 and Table 4, it can be concluded that monitoring local component failure is essential for low-code steel buildings across different storey heights, as there is no well-defined correlation between local component failures and global structural response. Also, evaluating the change in fragility using only global *EDP* (*MIDR*), can underestimate the system vulnerability for low-code buildings.

3B	Panel zone rotation		on (γ)		MIDR		
	med [g]		disp	med [g]		disp	
η %	LS3	% va <i>r</i>	LS3	LS3	% var	LS3	
0	0.417		0.316	0.449		0.343	
5	0.417	0.01%	0.316	0.441	1.7%	0.322	
10	0.372	10.8%	0.344	0.425	5.2%	0.336	
15	0.347	16.8%	0.335	0.386	13.9%	0.335	
20	0.331	20.7%	0.309	0.357	20.4%	0.335	
25	0.302	27.5%	0.347	0.310	30.9%	0.358	
30	0.276	33.8%	0.355	0.292	34.8%	0.362	
	Panel zone rotation (γ)			MIDR			
6B	Panel ze	one rotati	on (γ)		<i>MIDR</i>		
6B	Panel ze	one rotati	on (γ) disp	med [g]	MIDR	disp	
6B 		one rotati - % var	\# /	med [g]	<i>MIDR</i> % var	disp LS3	
	med [g]		disp				
η %	med [g] LS3		disp LS3	LS3		LS3	
$\frac{-\eta \%}{0}$	med [g] LS3 0.339	% var	<i>disp LS3</i> 0.349	LS3 0.347	% var	LS3 0.360	
η % 0 5	med [g] LS3 0.339 0.331	% var	disp LS3 0.349 0.347	LS3 0.347 0.358	% var	LS3 0.360 0.383	
η % 0 5 10	med [g] LS3 0.339 0.331 0.306	% var 2.6% 9.9%	disp LS3 0.349 0.347 0.364	LS3 0.347 0.358 0.358	% var	<i>LS3</i> 0.360 0.383 0.417	
η % 0 5 10 15	med [g] LS3 0.339 0.331 0.306 0.304	% var 2.6% 9.9% 10.3%	disp LS3 0.349 0.347 0.364 0.350	LS3 0.347 0.358 0.358 0.358	% var -3.3% -3.3% 4.4%	LS3 0.360 0.383 0.417 0.409	

9B	Panel zone rotation (γ)		MIDR			
	med [g]		disp	med [g]		disp
η %	LS3	% var	LS3	LS3	% var	LS3
0	0.192		0.575	0.267		0.647
5	0.198	-3.1%	0.584	0.240	10.1%	0.598
10	0.198	-3.1%	0.584	0.246	8.0%	0.609
15	0.201	-4.6%	0.535	0.230	13.7%	0.583
20	0.186	3.4%	0.550	0.235	12.0%	0.646
25	0.174	9.4%	0.554	0.233	12.9%	0.640
30	0.166	13.7%	0.553	0.235	12.0%	0.647

Table 4: Median (*med*) and the dispersion (*disp*) of the lognormal fragility curves for the as-built *vs.* the corroded frames for 3B, 6B, and 9B buildings.

6 CONCLUSIONS

The present study investigates the seismic performance of non-seismically designed (low-code) buildings with varying storey levels under the influence of atmospheric corrosion deterioration, considering different corrosivity categories. For this, benchmarked 3-, 6- and 9-storey steel Moment Resisting Frames (MRFs) are adopted from the literature. Atmospheric corrosion modelling, as per ISO 9223:2012, is adopted considering different corrosivity categories representing the varied intensity of corrosive environments. Consequently, a range of mass losses of 5% to 30% is selected for column sections over a 75-year period to model the corrosion damage. Finite Element (FE) models were developed in OpenSees for the as-built and corroded frames (for each mass loss) to perform non-linear time-history analyses. Atmospheric corrosion's primary and secondary effects were quantified and incorporated into the FE model. Incremental Dynamic Analyses (IDAs) are conducted through a suite of 30 records to evaluate seismic performance. The study monitors both global and local Engineering Demand Parameters (*EDPs*) to evaluate the performance under corrosion deterioration.

The results of the modal analyses revealed a slight elongation of the fundamental time period, reflecting stiffness degradation. Hence, for comparison purposes, average spectral acceleration is adopted as Intensity Measure (IM). Mass loss-based fragility curves are derived for the global and local-level EDPs considering code-based capacity limits (or limit state, LS). The fragility assessment reveals that panel zones (local *EDP*) govern the system fragility for all three steel MRFs (3-, 6- and 9-storey). The results show that global EDP can underestimate the failure probability for low-code steel MRFs. Furthermore, a consistent increase in fragility at the component level (panel zone) was observed with increasing mass loss, except for the 9-storey building for lower corrosion levels. However, for a given mass loss, the increase in fragility at the collapse limit state (LS3) was higher for the 3-storey building, while smaller variations were observed for 6- and 9-storey buildings. The results provide a good comparison of the evolution of seismic fragility with varying storey heights and increasing corrosion levels. The future works aim at constructing mass-loss based, time-independent, fragility functions for a portfolio of buildings, and studying the effect of storey heights on fragility functions of low- and mid-rise low-code steel buildings. This generic fragility function for building portfolios is an essential tool for estimating regional-scale seismic risk and provides detailed insights for policymakers, engineers, and stakeholders.

- [1] Mahin SA. Lessons from damage to steel buildings during the Northridge earthquake. Engineering Structures 1998;20:261–70.
- [2] Gutiérrez-Urzúa F, Freddi F. Influence of the design objectives on the seismic performance of steel moment resisting frames retrofitted with buckling restrained braces. Earthq Engng Struct Dyn 2022;51:3131–53.
- [3] Wang H, Wang Y, Zhang Z, Liu X, Xu S. Cyclic behavior and hysteresis model of beam-column joint under salt spray corrosion environment. Journal of Constructional Steel Research 2021;183:106737.
- [4] Zhang X, Zheng S, Zhao X. Experimental and numerical study on seismic performance of corroded steel frames in chloride environment. Journal of Constructional Steel Research 2020;171:106164.
- [5] Shekhar S, Ghosh J, Padgett JE. Seismic life-cycle cost analysis of ageing highway bridges under chloride exposure conditions: modelling and recommendations. Structure and Infrastructure Engineering 2018;14:941–66.
- [6] Shekhar S, Freddi F, Ghosh J, Lad D. Influence of corrosion on failure modes and lifetime seismic vulnerability assessment of low-ductility RC frames. Earthquake Engineering & Structural Dynamics 2023;52:5162–84.
- [7] Lekeufack BC, Fu B, Samuel MA, Alam S. Seismic resilience assessment of coastal carbon and weathering steel moment frame considering uniform atmospheric corrosion effects. Structures, vol. 69, Elsevier; 2024, p. 107274.
- [8] Di Sarno L, Majidian A, Karagiannakis G. The Effect of Atmospheric Corrosion on Steel Structures: A State-of-the-Art and Case-Study. Buildings 2021;11:571.
- [9] Lad D, Freddi F, Ghosh J, Rossetto T. Impact of corrosion deterioration on the seismic performance of steel frame structures, Society for Earthquake and Civil Engineering Dynamics (SECED); 2023.
- [10] Lad D, Freddi F, Ghosh J. Influence of atmospheric corrosivity on the seismic fragility of low-code steel frame structures, International Conference on Resilience, Earthquake Engineering and Structural Health Monitoring (ICONREM); 2024.
- [11]ISO 9223: 2012. Corrosion of metals and alloys—corrosivity of atmospheres—classification, determination and estimation. The British Standard Institute 2012.
- [12]McKenna F, Fenves GL, Scott MH, others. Open system for earthquake engineering simulation. University of California, Berkeley, CA 2000.
- [13] ISO 9224: 2012(E). Corrosion of Metals and Alloys Corrosivity of Atmospheres Guiding Values for the Corrosivity Categories. International Standards Organization, Geneve 2012.
- [14] Gupta A. Seismic demands for performance evaluation of steel moment resisting frame structures. Stanford University; 1999.
- [15] American Society of Civil Engineers. Minimum Design Loads and Associated Criteria for Buildings and Other Structures. ASCE/SEI 7-16. American Society of Civil Engineers; 2017.
- [16] Gutiérrez-Urzúa F, Freddi F, Di Sarno L. Comparative analysis of code-based approaches for seismic assessment of existing steel moment resisting frames. Journal of Constructional Steel Research 2021;181:106589.
- [17] Lignos DG, Krawinkler H. Deterioration Modeling of Steel Components in Support of Collapse Prediction of Steel Moment Frames under Earthquake Loading. J Struct Eng 2011;137:1291–302.
- [18] Zareian F, Medina RA. A practical method for proper modeling of structural damping in inelastic plane structural systems. Computers & Structures 2010;88:45–53.
- [19] Skiadopoulos A, Elkady A, Lignos DG. Proposed Panel Zone Model for Seismic Design of Steel Moment-Resisting Frames. J Struct Eng 2021;147:04021006.
- [20] Seismic Evaluation and Retrofit of Existing Buildings, ASCE/SEI 41-17. American Society of Civil Engineers; 2017.
- [21] Seismic Rehabilitation of Existing Buildings, ASCE/SEI 41-06. American Society of Civil Engineers; 2007.
- [22] Minimum Design Loads and Associated Criteria for Buildings and Other Structures,. ASCE/SEI 7-22. American Society of Civil Engineers; 2021.